

ON THE STABILITY OF SUPER EARTH ATMOSPHERES

KEVIN HENG^{1,3} AND PUSHKAR KOPPARLA²

Preprint: January 15, 2019

ABSTRACT

We investigate the stability of super Earth atmospheres around M stars using a 7-parameter, analytical framework. We construct stability diagrams in the parameter space of exoplanetary radius versus semi-major axis and elucidate the regions in which stable atmospheres may exist. We find that super Earth atmospheres with higher mean molecular weights and enhanced metallicities occupy a smaller region of allowed parameter space, because of the dual effects of diminished advection and enhanced radiative cooling. Furthermore, many super Earths which reside within the habitable zones of M stars may not possess stable, Earth-like atmospheres. We apply our stability diagrams to GJ 436b and GJ 1214b, and demonstrate that Earth-like elemental compositions for their atmospheres are disfavoured if these exoplanets possess solid surfaces and shallow atmospheres. Finally, we construct stability diagrams tailored to the *Kepler* dataset, for G and K stars, and predict that about half of the exoplanetary candidates are expected to harbour stable atmospheres if Earth-like conditions are assumed. We include 55 Cancri e and CoRoT-7b in our stability diagram for G stars.

Subject headings: planets and satellites: atmospheres

1. INTRODUCTION

The lower effective temperatures of M stars (or red dwarfs)—which comprise about three-quarters of the stellar population—render the detection of orbiting, close-in, Earth-like exoplanets amenable to both the transit and radial velocity techniques (Charbonneau 2009). The immense interest in hunting for exoplanets around these stars stems from the fact that the habitable zone is located at ~ 0.01 – 0.1 AU, rather than ~ 1 AU, away from these stars (Tarter et al. 2007). A consequence of the close proximity is that the exoplanets are expected to be tidally locked (or spin synchronized),⁴ meaning that they possess permanent dayside and nightside hemispheres. This expectation has led to theoretical concerns that the atmospheres may undergo collapse, because if heat is not redistributed efficiently from the dayside to the nightside it may lead to the dominant molecular species (e.g., CO₂, H₂O) condensing out on the nightside (e.g., Joshi, Haberle & Reynolds 1997; Joshi 2003). For example, Wordsworth et al. (2011) constructed three-dimensional, general circulation models tailored to the study of Gliese 581d and elucidated scenarios for atmospheric stability.

The discovery of close-in super Earths (e.g., Charbonneau et al. 2009) has generally inspired a number of theoretical studies of their possible atmospheres (e.g., Merlis & Schneider 2010; Rogers & Seager 2010; Castan & Menou 2011; Heng, Menou & Phillipps 2011; Heng & Vogt 2011; Heng, Frierson & Phillipps 2011; Pierrehumbert 2011; Valencia et al. 2011; Menou 2012), which either focus on specific case studies or explore a limited range of parameter space. In the present paper, we construct a simple, analytical framework to explore a broad range of parameter space describing the stability of super

Earth atmospheres. The key outcome of our study is the construction of a stability diagram, which allows one to judge if an exoplanetary atmosphere is likely to survive for a duration comparable to the age of its host star.

In §2, we describe our methodology. In §3, we present the basic stability diagram as well as variations of it applied to GJ 436b and GJ 1214b. In §4, we discuss the implications of our results and also apply our stability diagrams to the *Kepler* dataset of exoplanets and exoplanetary candidates, as well as 55 Cancri e and CoRoT-7b.

2. METHODOLOGY

To efficiently explore a wide range of parameter space, we construct a 7-parameter model with the following inputs:

1. The spatial separation between the exoplanet and its parent star (a);
2. The radius of the exoplanet (R);
3. The bulk mass density of the exoplanet (ρ_0);
4. The broadband opacity (κ_0), which is a proxy for the metallicity of the exoplanetary atmosphere;
5. The mean molecular weight of atmospheric atoms/molecules (μ);
6. The number of degrees of freedom of the atmospheric gas ($n_{\text{dof}} = 5$);
7. The Bond albedo of the exoplanetary atmosphere (A).

These basic parameters yield all of the other secondary parameters. We assume our exoplanets to be spherical, such that the mass is described by $M = 4\pi\rho_0 R^3/3$. The surface gravity is given by $g = 4\pi G\rho_0 R/3$, where G is the universal gravitational constant. The atmospheres are assumed to be thin, an assumption which we will elaborate on later. In addition, the stellar mass (M_\star), radius (R_\star) and effective temperature (T_\star) need to be specified.

¹ ETH Zürich, Institute for Astronomy, Wolfgang-Pauli-Strasse 27, CH-8093, Zürich, Switzerland

² ETH Zürich, Institute for Atmospheric and Climate Science, Universitätsstrasse 16, CH-8092, Zürich, Switzerland

³ Zwicky Prize Fellow

⁴ Strictly speaking, the terms “tidally locked” and “spin synchronized” are only synonymous for an exoplanet residing on a circular orbit. We use these terms interchangeably as we do not account for the effects of an eccentric orbit.

2.1. Stellar Irradiation and Orbital Parameters

The incident flux impinging upon the substellar point is

$$\mathcal{F}_0 = \sigma_{\text{SB}} T_{\text{irr}}^4, \quad (1)$$

where σ_{SB} is the Stefan-Boltzmann constant and the irradiation temperature is

$$T_{\text{irr}} = T_\star \left(\frac{R_\star}{a} \right)^{1/2} (1 - \mathcal{A})^{1/4}. \quad (2)$$

If one adopts parameter values appropriate to Earth (and $\mathcal{A} = 0$), one obtains the solar constant, $\mathcal{F}_0 \approx 1370 \text{ W m}^{-2}$.

Since the assumption of tidal locking is made, the orbital and rotational frequency are equal and given by

$$\Omega = \left(\frac{GM_\star}{a^3} \right)^{1/2}. \quad (3)$$

It is thus clear that T_{irr} (or \mathcal{F}_0) and Ω need to be varied self-consistently as one changes a .

2.2. Thermodynamics

The mean molecular mass $m = \mu m_{\text{H}}$ (with m_{H} denoting the mass of a hydrogen atom) and the number of degrees of freedom of the atmospheric gas n_{dof} collectively describe the thermodynamics and are manifested macroscopically via the adiabatic gas index,

$$\Gamma = 1 + \frac{2}{n_{\text{dof}}}, \quad (4)$$

as well as the adiabatic coefficient (Pierrehumbert 2010),

$$\kappa = \frac{2}{2 + n_{\text{dof}}} = \frac{\mathcal{R}}{c_P}, \quad (5)$$

where $\mathcal{R} = \mathcal{R}^*/\mu$ is the specific gas constant and $\mathcal{R}^* = 8314.5 \text{ J K}^{-1} \text{ kg}^{-1}$ is the universal gas constant. The sound speed is $c_s = (\Gamma k_{\text{B}} T_{\text{irr}}/m)^{1/2}$, where k_{B} is the Boltzmann constant. Furthermore, the specific heat capacity,

$$c_P = \frac{(2 + n_{\text{dof}}) \mathcal{R}^*}{2\mu}, \quad (6)$$

is used in evaluating the radiative time scale t_{rad} .

As an example, atmospheres dominated by molecular hydrogen have $\mu = 2$ and $n_{\text{dof}} = 5$, such that $\Gamma = 7/5$, $\kappa = 2/7$ and $\mathcal{R} = 4157.25 \text{ J K}^{-1} \text{ kg}^{-1}$. Dry, terrestrial air has a mean molecular weight of $\mu \approx 28.97$, such that $\mathcal{R} \approx 287 \text{ J K}^{-1} \text{ kg}^{-1}$. As a further example, we note that the model with $\mu \approx 17$ from Menou (2012) is termed “Water”, with relevance to a possible subclass of super Earths known as “water worlds” (Charbonneau et al. 2009; Rogers & Seager 2010; Bean et al. 2011). In practice, the effective number of degrees of freedom n_{dof} is not an integer (e.g., see Table 2.1, pg. 92, of Pierrehumbert 2010). For example, CO_2 has $n_{\text{dof}} \approx 6.8$, O_2 has $n_{\text{dof}} \approx 5.1$ and H_2 has $n_{\text{dof}} \approx 5.2$. For simplicity and to not obscure the salient physics of the model, we adopt $n_{\text{dof}} = 5$.

2.3. Atmospheric Opacity

At a basic level, the atmosphere is described by two broadband opacities: optical and infrared (see Heng et al. 2012 and references therein). We avoid this complication by assuming that the optical and infrared photospheres, as well as the photon deposition depth (Heng et al. 2012), are coincident and

thus may be described collectively by one broadband opacity (κ_0). This simplification implies that we are not accounting for the variation, with pressure, of the shortwave photosphere and photon deposition depth with the Bond albedo, and also any effects associated with clouds or hazes. Heng (2012) has shown (see Figure 5 of that study) that the efficiency of advection versus radiative cooling depends not only on irradiation, but also on the degree to which a temperature inversion is absent or present as well as the Bond albedo. Atmospheres with temperature inversions tend to be less advective and vertical turbulent mixing is also inhibited. A non-zero albedo in the shortwave generally shifts the photon deposition depth to higher altitudes and renders the atmosphere less advective. Given the current scarcity of knowledge on the atmospheric conditions on super Earths, we omit these refinements while being aware of them. For the rest of the paper, we refer to all three atmospheric layers simply as the “photosphere”.

The photosphere is located at a pressure where the optical depth is approximately unity,⁵

$$P = \frac{g}{\kappa_0}. \quad (7)$$

Invoking the ideal gas law yields an expression for the mass density of the atmosphere at the infrared photosphere,

$$\rho = \frac{mg}{\kappa_0 k_{\text{B}} T_{\text{irr}}} = \frac{1}{\kappa_0 H}. \quad (8)$$

Increasing the atmospheric opacity shifts the photosphere to higher altitudes, which mimics the effects of increased optical scattering and the presence of a temperature inversion.

2.4. Hydrodynamic Shallow Water Model

We utilize the linear, analytical, steady-state, two-dimensional version of the shallow water model of Showman & Polvani (2011) to model the photosphere of a super Earth. (See also Showman & Polvani 2010.) This model has been modified from the traditional shallow water models (e.g., Holton 2004; Vallis 2006) to treat the atmospheres of spin-synchronized exoplanets. (See also Heng & Spitkovsky 2009 and references therein.) Several adjustments are required to mimic the variation of various atmospheric quantities with the strength of stellar irradiation.

Firstly, we need to relate the mean shallow water height H to a characteristic height in the atmosphere, which we identify as the pressure scale height,

$$H = \frac{k_{\text{B}} T_{\text{irr}}}{mg}. \quad (9)$$

Secondly, we set the thermal forcing term S_0 (which has physical units of cm s^{-1}) to be H/t_0 , where $t_0 = (gH)^{-1/4} \beta^{-1/2}$ is the characteristic time scale used to non-dimensionalize the forcing and $\beta = 2\Omega/R$, and also adopt a zonal wave number of 0.5. In other words, the dimensionless forcing is set to be unity. The third ingredient is the radiative time scale

⁵ In the classical Milne solution for gray, stellar atmospheres, the photosphere is located at an optical depth of $\tau = 2/3$ because the temperature is equal to the effective stellar temperature (T_\star) at this layer (Mihalas 1978). In cool ($T_{\text{irr}} \ll T_{\text{int}}$) exoplanetary atmospheres, $\tau = 2/3$ specifies the atmospheric layer where the temperature is equal to the *internal temperature* (T_{int}). In general, determining the value of τ corresponding to the photosphere involves solving for the atmospheric layer where the temperature is equal to the equilibrium temperature (with an order of unity correction related to heat redistribution), i.e., enforcing the conservation of energy.

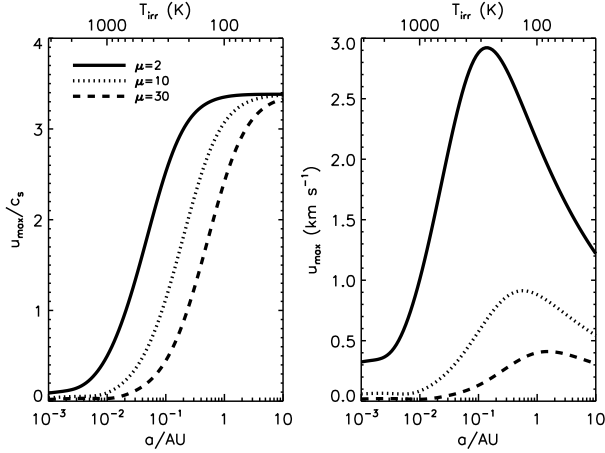


FIG. 1.— Variation of the maximum zonal wind speed, non-dimensionalized (left panel) and in physical units (right panel), with a (or T_{irr}), computed using the shallow water model of Showman & Polvani (2011) which is specialized to tidally-locked exoplanets. For illustration, we adopt $M_\star = 0.184 M_\odot$, $R_\star = 0.203 R_\odot$ and $T_\star = 3240$ K (appropriate to a M3.5 star) as well as $\mathcal{A} = 0$. Shown also are the curves for different values of the mean molecular weight μ .

(Goody & Yung 1989), which is the ratio of the thermal energy content per unit area ($c_P T_{\text{irr}} \tilde{m}$ where $\tilde{m} = P/g$ is the column mass in hydrostatic equilibrium) to the flux \mathcal{F}_0 ,

$$t_{\text{rad}} = \frac{c_P}{\sigma_{\text{SB}} \kappa_0 T_{\text{irr}}^3}, \quad (10)$$

which enters into the momentum equations via a radiative drag term ($-\vec{v}/t_{\text{rad}}$).

The fourth—and most uncertain—ingredient is the hydrodynamic drag time scale, which we set to be the rotational/orbital period,

$$t_{\text{drag}} = \frac{2\pi}{\Omega}. \quad (11)$$

On Earth, the source of hydrodynamic drag originates from the boundary layer (Garraff 1994), which is the transition region from a “no slip” to a “free slip” condition between the atmosphere and the terrestrial surface. In the Held-Suarez benchmark test for Earth, the time scale for Rayleigh drag is set to be one Earth day (Held & Suarez 1994). Our simple assumption for t_{drag} is plausible and commensurate with the fact that the true source of drag in super Earth atmospheres remains to be identified. Even the simplest implementation of a boundary layer scheme for Earth (Troen & Mahrt 1986; Frierson, Held & Zurita-Gotor 2006) requires the specification of four additional parameters, which is currently unjustified given the dearth of astronomical information on this issue.

2.5. Basic Trends with Strength of Stellar Irradiation

To assess the efficiency of heat redistribution from the day-side to the nightside hemisphere of a tidally-locked super Earth, one needs to compare the radiative to the advective time scale (Showman & Guillot 2002). Perna, Heng & Pont (2012) have shown using three-dimensional simulations of atmospheric circulation—albeit in the context of hot Jupiters—that a reasonable approach to computing the advective time scale is to evaluate

$$t_{\text{adv}} \sim \frac{R}{u_{\text{max}}}, \quad (12)$$

where $u_{\text{max}} \equiv \max\{u\}$ and u is the zonal wind speed.

While we do not expect the shallow water model of Showman & Polvani (2011) to reproduce all of the trends obtained from the three-dimensional simulations, we do expect u_{max} to generally increase with T_{irr} when hydrodynamic drag is insignificant. The right panel of Figure 1 confirms this expectation for $a \gtrsim 0.1$ AU, a basic trend which is supported by the results obtained from three-dimensional simulations of atmospheric circulation (e.g., Perna, Heng & Pont 2012). At $a \lesssim 0.1$ AU, the hydrodynamic drag condition we have imposed to mimic the effects of the boundary layer sets in and reverses the trend. We have checked that if t_{drag} is kept constant (and at a large value), then u_{max} increases monotonically with decreasing a . The left panel of Figure 1, which shows the maximum zonal wind speed normalized by the sound speed, illustrates the effects of hydrodynamic drag more succinctly.

The model also predicts that u_{max} decreases when the mean molecular weight increases, because a larger value of μ corresponds to stronger radiative forcing (i.e., shorter t_{rad}). Such a trend with μ is consistent with the simulated results of Menou (2012), who—by examining models for GJ 1214b with $\mu \approx 2, 3$ and 17—found that a higher value of μ leads to a higher ratio of dayside to nightside photospheric flux, implying that heat redistribution becomes less efficient as μ increases. In other words, a “heavier” atmosphere (either through a higher value of μ or κ_0) tends to be both less advective and more radiative. We have checked that the qualitative trends in our stability diagrams are similar whether we adopt $t_{\text{drag}} = 2\pi/\Omega$ or as a constant, arbitrary value, although the quantitative results do differ.

2.6. Inefficiency of Thermal Conduction

We assume that the rocky cores of our model super Earths do not efficiently conduct enough heat from the irradiated dayside hemisphere to the cold nightside hemisphere to prevent atmospheric collapse. We will now demonstrate that this is a plausible assumption.

In one dimension, the conduction equation reads

$$\frac{\partial T}{\partial t} = \alpha_0 \frac{\partial^2 T}{\partial x^2}, \quad (13)$$

where T denotes the temperature, t the time, x the spatial coordinate and

$$\alpha_0 = \frac{k_{\text{cond}}}{\rho_0 c_{P_0}} \quad (14)$$

is the thermal diffusivity of the material of the rocky core. Here, c_{P_0} denotes the specific heat capacity, at constant pressure, of the rocky core (and not the atmosphere). Assuming that $T = T(x, t) = T_x(x)T_t(t)$ is a separable function of x and t yields

$$\frac{dT_t}{dt} = -C\alpha_0 T_t, \quad (15)$$

which has the solution

$$T_t = T_{t_0} \exp(-C\alpha_0 t), \quad (16)$$

where $T_{t_0} \equiv T_t(t = 0)$ and $-C$ is the separation constant. We identify $C = 1/R^2$, such that the characteristic thermal conduction time scale is

$$\begin{aligned} t_{\text{cond}} &= \frac{\rho_0 c_{P_0} R^2}{k_{\text{cond}}} \\ &\approx 4 \times 10^7 \text{ yr} \left(\frac{\rho_0}{3 \text{ g cm}^{-3}} \frac{c_{P_0}}{10^7 \text{ erg K}^{-1} \text{ g}^{-1}} \right) \\ &\quad \times \left(\frac{R}{R_\oplus} \right)^2 \left(\frac{k_{\text{cond}}}{10^{10} \text{ erg K}^{-1} \text{ s}^{-1}} \right)^{-1}. \end{aligned} \quad (17)$$

Rocky material is expected to have a thermal conductivity of $k_{\text{cond}} \sim 1 \text{ W m K}^{-1} = 10^{10} \text{ erg K}^{-1} \text{ s}^{-1}$ and a specific heat capacity of $c_{P_0} \sim 10^7 \text{ erg K}^{-1} \text{ g}^{-1}$. Demanding that the radiative cooling time is less than the thermal conduction time yields the condition

$$T > \left(\frac{k_{\text{cond}}}{\sigma_{\text{SB}} R} \right)^{1/3} \approx 65 \text{ K} \left(\frac{k_{\text{cond}}}{10^{10} \text{ erg K}^{-1} \text{ s}^{-1}} \right)^{1/3} \left(\frac{R}{R_{\oplus}} \right)^{-1/3}. \quad (18)$$

The condition in equation (18) implies that as long as the rocky surfaces of close-in super Earths are heated to $\gtrsim 100 \text{ K}$, thermal conductivity will not operate rapidly enough to heat the cold nightside hemisphere. The possibility of significant geothermal heating from the core is not considered in our models and remains a topic for future investigation.

3. STABILITY DIAGRAMS

3.1. Conditions Related to Advection & Radiation

Since the atmosphere is predominantly forced by stellar irradiation, the main effect is the competition between advection and radiative cooling. A plausible, necessary condition for atmospheric stability is $t_{\text{adv}} < t_{\text{rad}}$, which yields

$$R < \left(\frac{c_P u_{\text{max}}}{\sigma_{\text{SB}} \kappa_0} \right) T_{\star}^{-3} R_{\star}^{-3/2} (1 - \mathcal{A})^{-3/4} a^{3/2}. \quad (19)$$

The maximum zonal wind speed, u_{max} , is obtained from our shallow water model (see §2.4). A reasonable approximation to the condition in equation (19) is to set $u_{\text{max}} = c_s$, which yields

$$R < \left(\frac{\Gamma k_B}{m} \right)^{1/2} \left(\frac{c_P}{\sigma_{\text{SB}} \kappa_0} \right) \times T_{\star}^{-5/2} R_{\star}^{-5/4} (1 - \mathcal{A})^{-5/8} a^{5/4}. \quad (20)$$

Since free gravity waves have a speed $\sim c_s$, the condition in equation (20) may also be interpreted as a constraint on heat redistribution mediated by free gravity waves.

We have made the assumption that if convective instability is triggered, it leads to the redistribution of heat primarily in the vertical and meridional directions (and not in the zonal direction), which is corroborated by three-dimensional simulations of atmospheric circulation for tidally-locked, Earth-like exoplanets (Joshi 2003; Merlis & Schneider 2010; Heng & Vogt 2011; Heng, Frierson & Phillips 2011).

3.2. Conditions Related to Orbital Circularization & Spin Synchronization

Our application of the Showman & Polvani (2011) shallow water model breaks down—and the concerns about atmospheric stability are alleviated or even obviated—if the exoplanet is not spin-synchronized, but still (approximately) applies if it resides on a mildly eccentric orbit.⁶ (See Laughlin et al. 2009 for an illustration of the effects of stellar irradiation on the atmosphere of an exoplanet residing on a highly eccentric, but spin-synchronized, orbit.) The time scale associated with spin synchronization is (Bodenheimer, Lin & Mardling 2001)

$$t_{\text{syn}} = \frac{8Q}{45\Omega} \left(\frac{\omega}{\Omega} \right) \left(\frac{M}{M_{\star}} \right) \left(\frac{a}{R} \right)^3, \quad (21)$$

⁶ We will see later that the $t_{\text{adv}} = t_{\text{rad}}$ and the $t_{\text{circ}} = t_{\star}$ lines typically do not intersect.

where ω is the *rotational* frequency of an exoplanet which is not initially spin-synchronized. The time scale associated with the circularization of the orbit is (Goldreich & Soter 1966)

$$t_{\text{circ}} = \frac{4Q}{63\Omega} \left(\frac{M}{M_{\star}} \right) \left(\frac{a}{R} \right)^5. \quad (22)$$

In both equations (21) and (22), the tidal quality factor is $Q = 2\pi E_{\text{peak}}/\Delta E$, where E_{peak} is the peak tidal energy stored and ΔE is the amount of energy dissipated per forcing cycle (Knopoff 1964; Goldreich & Soter 1966; Bodenheimer, Lin & Mardling 2001). Following Knopoff (1964) and Goldreich & Soter (1966), we adopt $Q = 10$ –100 for rocky exoplanets. Spin synchronization generally occurs faster than orbital circularization, unless

$$a < R \sqrt{\frac{14}{5} \left(\frac{\omega}{\Omega} \right)}. \quad (23)$$

If $\omega/\Omega = 100$, then the numerical coefficient in equation (23) is about 17. This condition appears unlikely to be satisfied. Demanding that $t_{\text{syn}} < t_{\star}$ and $t_{\text{circ}} < t_{\star}$ yield a pair of respective conditions:

$$a < \left(\frac{135t_{\star}}{32\pi Q \rho_0} \right)^{2/9} \left(\frac{\Omega}{\omega} \right)^{2/9} G^{1/9} M_{\star}^{1/3}, \quad (24)$$

$$R > \left(\frac{16\pi Q \rho_0}{189t_{\star}} \right)^{1/2} G^{-1/4} M_{\star}^{-3/4} a^{13/4}.$$

A caveat is that if the exoplanet ends up in 1 : N tidal resonances where $N > 1$, then this tends to homogenize the zonal temperature differences, thus further alleviating concerns about atmospheric collapse (Wordsworth et al. 2011).

3.3. Other Conditions

In order to retain its atmosphere, a super Earth needs to possess a radius which is larger than its Hill sphere $R_{\text{H}} = a(M/3M_{\star})^{1/3}$, which implies that

$$a > \left(\frac{9M_{\star}}{4\pi \rho_0} \right)^{1/3}. \quad (25)$$

The thermal speed ($\sim c_s$) of the atmospheric gas also needs to not exceed the escape speed of the exoplanet, $v_{\text{esc}} = (2GM/R)^{1/2}$,

$$R > \left(\frac{3\Gamma k_B}{8\pi G \rho_0 m} \right)^{2/3} T_{\star}^{2/3} (1 - \mathcal{A})^{1/6} a^{-1/3}. \quad (26)$$

3.4. Basic Stability Diagram

Figure 2 shows the basic stability diagram for super Earth atmospheres in the parameter space of R versus a . For the condition $t_{\text{syn}} < t_{\star}$, we have used $\omega/\Omega = 100$ merely as an illustration. As expected, the condition $R/c_s < t_{\text{rad}}$ is less constraining than $t_{\text{adv}} < t_{\text{rad}}$ across all of the considered values of R , a and μ ; reassuringly, both conditions produce similar qualitative trends. The condition $R_{\text{H}} > R$ is overwhelmed by both the $t_{\text{adv}} < t_{\text{rad}}$ and $v_{\text{esc}} > c_s$ conditions. A key feature of Figure 2 is that atmospheres with lower mean molecular weights (μ) tend to occupy a larger allowed region of parameter space.

We include in Figure 2 the measured values of R and a for GJ 436b and GJ 1214b. For GJ 436b, we use the values of $R \approx 3.96R_{\oplus}$ and $a \approx 0.0287 \text{ AU}$ as reported by

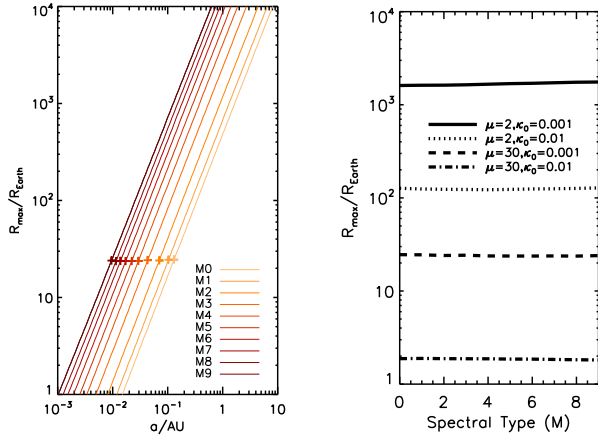


FIG. 4.— Maximum exoplanetary radius R_{\max} allowed by the $t_{\text{adv}} < t_{\text{rad}}$ condition across the spectral types M0 to M9. The left panel shows the set of R_{\max} curves, versus a , for $\mu = 30$ and $\kappa_0 = 0.001 \text{ cm}^2 \text{ g}^{-1}$. The crosses mark the location of the center of the habitable zone for each spectral type. The right panel shows the R_{\max} value corresponding to the center of each habitable zone as a function of the spectral type and for different combinations of the mean molecular weight μ and atmospheric opacity κ_0 .

remain controversial (Rogers & Seager 2010; Bean et al. 2011; Croll et al. 2011; Désert et al. 2011; de Mooij et al. 2012; Miller-Ricci Kempton, Zahnle & Fortney 2012), including the possibility that a reduced value of the radius—which may obtain from an updated estimate of the distance to GJ 1214 via improved parallax measurements—is consistent with an atmosphere-less exoplanet. Detecting or ruling out the presence of a Rayleigh scattering slope in the spectrum at shorter wavelengths is a valuable atmospheric diagnostic for μ (de Mooij et al. 2012).

As a word of caution, we note that it is yet unknown if either GJ 436b or GJ 1214b possess solid surfaces within their gaseous atmospheres. If these exoplanets are more similar to gas giants—or possess thick atmospheres enveloping a solid core, such that the deeper layers are advective despite the shallower layers being predominantly radiative—then the conditions on atmospheric stability simply translate into conditions for the efficiency of heat redistribution with no catastrophic consequences for the atmospheres (Joshi, Haberle & Reynolds 1997). This basic expectation is consistent with the results obtained from the three-dimensional simulations of Wordsworth et al. (2011), who find thicker atmospheres to be more stable (albeit within the context of exploring atmospheric scenarios for Gliese 581d). From another perspective, our use of the adjective “thick” is akin to positing the presence of a greenhouse effect which is substantial enough to counteract the inadequacy of (poor) advection.

4. DISCUSSION

The theory of (exo)planet formation remains fraught with uncertainties. Therefore, an attempt to construct a formation model for super Earth atmospheres—which are probably secondary (i.e., due to outgassing) and unlikely to reflect the elemental compositions of the primordial nebulae from which they formed—remains an unconstrained exercise in some instances (e.g., Miguel et al. 2011). From this perspective, our analytical framework may be regarded as a survival—rather than formation—model, similar to what has been constructed for planetesimal disks (Heng & Tremaine 2010).

We have posited that inefficient advection from the dayside

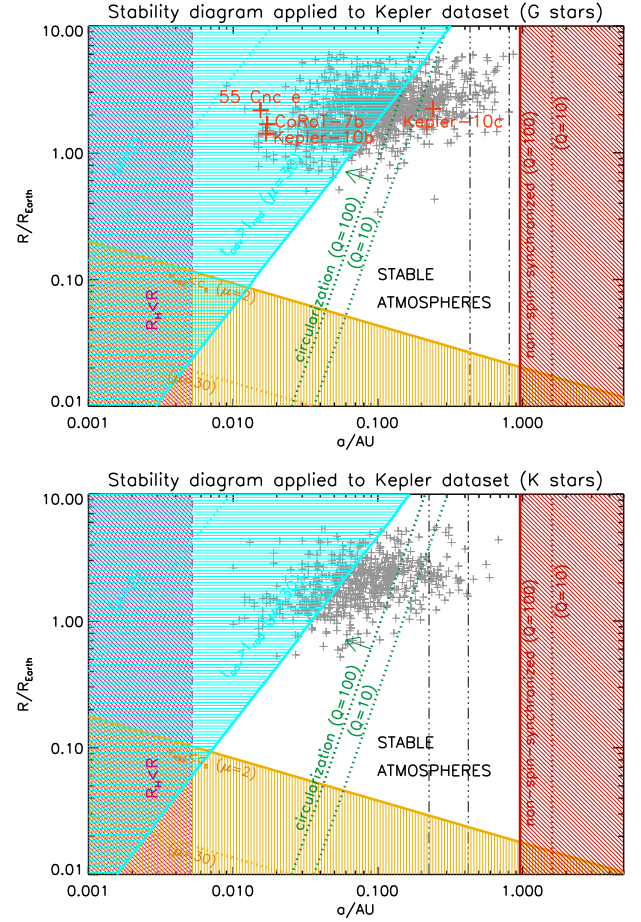


FIG. 5.— Basic stability diagrams applied to the *Kepler* dataset for G (top panel; 1135 objects) and K (bottom panel; 613 objects) stars. The photospheric pressure is assumed to be $P \sim 1$ bar in these diagrams (see text). The triple-dot-dash lines denote the boundaries of the habitable zones. For the stability diagram applied to G stars, we include 55 Cancri e and CoRoT-7b as well as highlighting Kepler-10b and Kepler-10c.

to the nightside of a tidally-locked exoplanet causes the major atmospheric constituents to condense out on the nightside, but we have not elucidated the details of this phase change. Thus, the $t_{\text{adv}} < t_{\text{rad}}$ condition should strictly be viewed as a necessary but generally insufficient condition. Our hope is that our simple framework will motivate future work on a broad range of atmospheric constituents and not just Earth- or even Solar System-centric ones. More refined trains of thought include the consideration of feedback mechanisms such as the water ice-albedo feedback, which has been shown to operate weakly on tidally-locked exoplanets with Earth-like stellar irradiation and atmospheric conditions (Joshi, Haberle & Reynolds 1997; Joshi 2003).

Our basic stability diagram (Figure 2) demonstrates that there is a maximum exoplanetary radius R_{\max} above which the (thin) atmospheres of super Earths are unstable. In the left panel of Figure 4, we show R_{\max} as a function of a across the spectral types M0 to M9. The less intensive irradiation from the cooler M stars leads to more lethargic radiative cooling in the atmospheres of their super Earths, which increases R_{\max} across all values of a . However, this effect is offset by the center of the habitable zone moving inwards, towards the star, for later spectral types. The collective result is that R_{\max} is insensitive to the spectral type. Rather, it is somewhat sensitive to the mean molecular weight (μ) and metallicity (via the

opacity κ_0), as shown in the right panel of Figure 4. Atmospheres with enhanced metallicities and higher mean molecular weights have lower values of R_{\max} , implying that the condition for stability is more stringent. For Earth-like atmospheres ($\mu = 30$) and $g \sim 10 \text{ m s}^{-2}$, the photospheres of super Earths with $R \sim 1\text{--}10R_{\oplus}$ need to be located at $P \gtrsim 1$ bar for stability.

As a final demonstration of the power of our stability diagram, we apply it to the *Kepler* dataset (Borucki et al. 2011; Batalha et al. 2012). We include all exoplanets and exoplanet candidates with $R < 6R_{\oplus}$. We construct two diagrams for G ($5200 \text{ K} < T_{\star} \leq 6000 \text{ K}$) and K ($3700 \text{ K} < T_{\star} \leq 5200 \text{ K}$) stars using the average values of the stellar parameters for each sub-sample. We adopt $t_{\star} = 5 \text{ Gyr}$ for illustration, noting that this only affects the conditions on circularization and spin synchronization. In the absence of empirical constraints, we adopt Solar System-centric values for various parameters ($\rho_0 = 3 \text{ g cm}^{-3}$, $\mathcal{A} = 0.3$), but note that our estimates are insensitive to these assumptions. A key, unknown parameter is the broadband atmospheric opacity. In Figure 5, we set $\kappa_0 = 0.001 \text{ cm}^2 \text{ g}^{-1}$ such that the photospheric pressure is $P = g/\kappa_0 \sim 1 \text{ bar}$ for $g \sim 10 \text{ m s}^{-2}$. With $P \sim 1 \text{ bar}$, all of the 1135 *Kepler* exoplanets and exoplanetary candidates orbiting G stars have stable atmospheres if the atmospheres are dominated by molecular hydrogen ($\mu = 2$), whereas $494/1135 \approx 44\%$ of them have stable atmospheres if they are Earth-like in composition ($\mu = 30$). For $P \sim 0.1 \text{ bar}$, these percentages become about 93% and 0.4%, respectively. For $P \sim 10 \text{ bar}$, they become 100% and 99%, respectively.

We include in the stability diagram for G stars the measured R and a values for 55 Cancri e ($R \approx 2.17R_{\oplus}$, $a \approx 0.01544 \text{ AU}$; Demory et al. 2011; Gillion et al. 2012) and CoRoT-7b ($R \approx 1.68R_{\oplus}$, $a \approx 0.0172 \text{ AU}$; Léger et al. 2009). We also highlight the exoplanets Kepler-10b ($R \approx 1.416R_{\oplus}$,

$a \approx 0.01684 \text{ AU}$; Batalha et al. 2011) and Kepler-10c ($R \approx 2.227R_{\oplus}$, $a \approx 0.2407 \text{ AU}$; Fressin et al. 2011). It remains possible that 55 Cancri e, CoRoT-7b and Kepler-10b may maintain minimal atmospheres—which do not extend beyond the day-night terminators and are dynamically dominated by vertical, rather than horizontal, flows—established through vapour saturation equilibrium with their continuously eroded rocky surfaces (Castan & Menou 2011; Valencia et al. 2011).

For the K stars (613 exoplanets and exoplanet candidates), we obtain similar numbers: for $P \sim 0.1 \text{ bar}$, we get 98% ($\mu = 2$) and 2% ($\mu = 30$); for $P \sim 1 \text{ bar}$, we get 100% ($\mu = 2$) and 69% ($\mu = 30$); for $P \sim 10 \text{ bar}$, we get 100% ($\mu = 2$) and 99.7% ($\mu = 30$). Curiously, the exoplanet candidates and exoplanets residing within the habitable zones of both the *Kepler* G and K stars are likely to possess stable atmospheres, unlike the situation with M stars.

If these exoplanetary atmospheres are Earth-like ($P \sim 1 \text{ bar}$, $\mu \approx 30$), then about half of them are expected to be stable. The continued expansion of the *Kepler* dataset and the eventual, inexorable pursuit of follow-up observations to further characterize these exoplanets will allow our predictions to be tested. For example, the photospheric infrared emission from atmosphere-less super Earths is likely to be emanated directly from their rocky surfaces, such that the dayside to nightside flux contrast will appear marked; these exoplanets will also exhibit flat transmission spectra.

KH acknowledges generous support by the Zwicky Prize Fellowship of ETH Zürich (Star and Planet Formation Group; PI: Michael Meyer). We are grateful to Sascha Quanz and George Lake for illuminating conversations, as well as Jonathan Mitchell for stimulating comments which improved the clarity and quality of the manuscript.

REFERENCES

- Batalha, N.M., et al. 2011, *ApJ*, 729, 27
 Batalha, N.M., et al. 2012, preprint (arXiv:1202.5852)
 Bean, J.L., et al. 2011, *ApJ*, 743, 92
 Bodenheimer, P., Lin, D.N.C., & Mardling, R.A. 2001, *ApJ*, 548, 466
 Borucki, W.J., et al. 2011, *ApJ*, 736, 19
 Carter, J.A., Winn, J.N., Holman, M.J., Fabrycky, D., Berta, Z.K., Burke, C.J., & Nutzman, P. 2011, *ApJ*, 730, 82
 Castan, T., & Menou, K. 2011, *ApJ*, 743, L36
 Charbonneau, D. 2009, Proceedings of the IAU Symposium, eds. F. Pont, D. Sasselov & M. Holman, 253, pg. 1–8
 Charbonneau, D., et al. 2009, *Nature*, 462, 891
 Croll, B., Albert, L., Jayawardhana, R., Miller-Ricci Kempton, E., Fortney, J.J., Murray, N., & Neilson, H. 2011, *ApJ*, 736, 78
 de Mooij, E.J.W., et al. 2012, *A&A*, 538, A46
 Demory, B.-O., et al. 2011, *A&A*, 533, 114
 Désert, J.-M., et al. 2011, *ApJ*, 731, L40
 Ehrenreich, D., & Désert, J.-M. 2011, *A&A*, 529, A136
 Fressin, F., et al. 2011, *ApJS*, 197, 5
 Frierson, D.M.W., Held, I.M., & Zurita-Gotor, P. 2006, *Journal of the Atmospheric Sciences*, 63, 2548
 Garratt, J.R. 1994, *Earth-Science Reviews*, 37, 89
 Gillon, M., et al. 2012, *A&A*, 539, A28
 Goldreich, P., & Soter, S. 1966, *Icarus*, 5, 375
 Goody, R.M., & Yung, Y.L. 1989, *Atmospheric radiation: theoretical basis*, 2nd edition (New York: Oxford University Press)
 Held, I.M., & Suarez, M.J. 1994, *Bulletin of the American Meteorological Society*, 75, 1825
 Heng, K., & Spitkovsky, A. 2009, *ApJ*, 703, 1819
 Heng, K., & Tremaine, S. 2010, *MNRAS*, 401, 867
 Heng, K., Menou, K., & Philipps, P.J. 2011, *MNRAS*, 413, 2380
 Heng, K., & Vogt, S.S. 2011, *MNRAS*, 415, 2145
 Heng, K., Frierson, D.M.W., & Philipps, P.J. 2011, *MNRAS*, 418, 2669
 Heng, K., Hayek, W., Pont, F., & Sing, D.K. 2012, *MNRAS*, 420, 20
 Heng, K. 2012, *ApJ*, 748, L17
 Holton, J.R. 2004, *An Introduction to Dynamic Meteorology*, 4th edition (Massachusetts: Elsevier)
 Joshi, M.M., Haberle, R.M., & Reynolds, R.T. 1997, *Icarus*, 129, 450
 Joshi, M. 2003, *Astrobiology*, 3, 415
 Kite, E.S., Gaidos, E., & Manga, M. 2011, *ApJ*, 743, 41
 Knopoff, L. 1964, *Reviews of Geophysics*, 2, 625
 Knutson, H.A., et al. 2011, *ApJ*, 735, 27
 Laughlin, G., Deming, D., Langton, J., Kasen, D., Vogt, S., Butler, P., Rivera, E., & Meschiari, S. 2009, *Nature*, 457, 562
 Léger, A., et al. 2009, *A&A*, 506, 287
 Menou, K. 2011, *ApJ*, 744, L16
 Merlis, T.M., & Schneider, T. 2010, *Journal of Advances in Modeling Earth Systems — Discussion (JAMES-D)*, 2, 13
 Miguel, Y., Kaltenegger, L., Fegley, B., & Schaefer, L. 2011, *ApJ*, 742, L19
 Mihalas, D. 1978, *Stellar Atmospheres*, 2nd edition (San Francisco: Freeman)
 Miller-Ricci Kempton, E., Zahnle, K., & Fortney, J.J. 2012, *ApJ*, 745, 3
 Perna, R., Heng, K., & Pont, F. 2012, preprint (arXiv:1201.5391v1)
 Pierrehumbert, R.T. 2010, *Principles of Planetary Climate* (New York: Cambridge University Press)
 Pierrehumbert, R.T. 2011, *ApJ*, 726, L8
 Rogers, L.A., & Seager, S. 2010, *ApJ*, 716, 1208
 Showman, A.P., & Guillot, T. 2002, *A&A*, 385, 166
 Showman, A.P., & Polvani, L.M. 2010, *Geophysical Research Letters*, 37, L18811
 Showman, A.P., & Polvani, L.M. 2011, *ApJ*, 738, 71
 Tarter, J., et al. 2007, *Astrobiology*, 7, 30
 Troen, I.B., & Mahrt, L. 1986, *Boundary-Layer Meteorology*, 37, 129
 Wordsworth, R.D., Forget, F., Selsis, F., Millour, E., Charnay, B., & Madeleine, J.-B. 2011, *ApJ*, 733, L48
 Valencia, D., Ikoma, M., Guillot, T., & Nettelmann, N. 2011, *A&A*, 516, A20
 Vallis, G.K. 2006, *Atmospheric and Oceanic Fluid Dynamics: Fundamentals and Large-Scale Circulation* (New York: Cambridge University Press)